Investigating the role of background and observation error correlations in improving a model forecast of forest carbon balance using 4D-Var.

Ewan Pinnington add authors and affiliations

November 8, 2015

Abstract

Efforts to implement variational data assimilation routines with functional ecology and land surface models have been limited with sequential and Markov chain Monte Carlo data assimilation methods being more prevalent. When data assimilation has been used with models of carbon balance, background errors (describing our knowledge of error in our prior model estimates before data assimilation) and observation errors have largely been treated as independent and uncorrelated. In numerical weather prediction it has been shown that including correlations in these errors can considerably improve data assimilation results and forecasts. In this paper we implement a four-dimensional Variational data assimilation scheme with a simple model of forest carbon balance, for joint parameter and state estimation, assimilating observations of Net Ecosystem Exchange (NEE) taken at the Alice Holt flux site in Hampshire, UK managed by Forest Research. We then investigate the effect of specifying correlations between parameter and state variables in background error statistics and the effect of specifying correlations in time between observation error statistics. In data assimilation background and observation error statistics are often described by the background error covariance matrix and the observation error covariance matrix. We outline novel methods for creating correlated versions of these matrices, using a set of dynamical constraints to include correlations in the background error statistics and a gaussian correlation function to include time correlations in the observation error statistics. We show that using these new correlated matrices can almost halve the root mean square error in our models forecast of NEE in comparison to the results when using uncorrelated diagonal background and observation error covariance matrices, going from 4.22gCm^{-2}day^{-1} to 2.38gCm^{-2}day^{-1}.

1 Introduction

Terrestrial ecosystems and oceans are responsible for removing around half of all human emitted carbon-dioxide from the atmosphere and therefore mediate the effect of anthropogenic induced climate change [Ciais et al., 2014]. Terrestrial ecosystem carbon uptake is the least understood process in the global carbon cycle. It is therefore vital that we improve understanding of the carbon uptake of terrestrial ecosystems and their response to climate change in order to better constrain predictions of future carbon budgets. Observations of the Net Ecosystem Exchange (NEE) of CO_2 between terrestrial ecosystems and the atmosphere are now routinely made at flux tower sites world-wide [Baldocchi, 2008] providing a valuable resource for model validation and data assimilation.

Data assimilation is the process of combining a mathematical model with observations in order to improve the estimate of the state of a system. Data assimilation has successfully been used in many applications to significantly improve model state and forecasts. Perhaps the most important application has been in numerical weather prediction where the impact of data assimilation has been that the four day forecast in 2014 has the same level of accuracy as the one day forecast in 1979 [Bauer et al., 2015].

This increase in forecast skill is obviously not solely due to data assimilation but also increased quality and resolution of observations along with improvements in model structure, however the introduction and evolution of data assimilation has played a large part [Dee et al., 2011]. The current method implemented at many leading operational numerical weather prediction centres is known as Four-Dimensional Variational data assimilation (4D-Var) [Rabier et al., 2000, Rawlins et al., 2007], which has been shown to be a significant improvement over its predecessor three-dimensional variational assimilation [Lorenc and Rawlins, 2005]. Variational assimilation techniques minimise a cost function to find the optimal state of a system given all available knowledge of errors in the model and observations. The minimisation routine typically requires the derivative of the model, this can sometimes prove difficult to calculate. Using techniques such as automatic-differentiation can reduce the time taken to implement the derivative of a model. In numerical weather prediction data assimilation has been predominately used for state estimation whilst keeping parameters fixed. Variational data assimilation can be used for joint parameter and state estimation by augmenting the parameters into the state vector [Navon, 1998]. By including the parameters in the state vector we must also specify error statistics and error correlations for them. In Smith et al. [2009] it is shown that the prescription of these error statistics and their correlations can have a significant impact on parameter-state estimates obtained from the assimilation.

Many different observations relevant to the carbon balance of forests have now been combined with functional ecology models, using data assimilation, in order to improve our knowledge ecological systems [Fox et al., 2009, Niu et al., 2014, Quaife et al., 2008, Richardson et al., 2010, Zobitz et al., 2014, 2011]. Two such models that have been used extensively with data assimilation are the Data Assimilation Linked Ecosystem Carbon (DALEC) model [Williams et al., 2005] and the Simplified Photosynthesis and Evapo-Transpiration (SIPNET) model [Braswell et al., 2005]. Nearly all data assimilation routines built with these models have used sequential and Monte Carlo Markov chain (MCMC) data assimilation methods with the exception of DALEC being implemented in a variational routine by Delahaies et al. [2013]. There have been examples of global land surface models being implemented with variational methods such as the Carbon Cycle Data Assimilation System (CCDAS) [Kaminski et al., 2013] and the ORganizing Carbon and Hydrology In Dynamic EcosystEms model (ORCHIDEE) [Krinner et al., 2005]. These examples have mainly been used to assimilate data from satellite observations with a few examples where site level data has been assimilated [Bacour et al., 2015, Verbeeck et al., 2011].

Background errors (describing our knowledge of error in our prior model estimates before data assimilation) and observation errors have largely been treated as uncorrelated and independent in ecosystem model data assimilation schemes. In 3D and 4DVar schemes background and observation errors are represented by the error covariance matrices $\mathbf{B}$ and $\mathbf{R}$ respectively. The off-diagonal elements of these matrices indicate the correlations between the parameter and state variables for $\mathbf{B}$ and the correlations between observation errors for $\mathbf{R}$. In the assimilation the off-diagonal terms in the $\mathbf{B}$ matrix act to spread information between the state and augmented parameter variables [Kalnay, 2003]. This means that assimilating observations of one state variable can act to update different state variables in the assimilation when correlations are included in $\mathbf{B}$. In 4D-Var the $\mathbf{B}$ matrix is propagated implicitly by the forecast model, so that even a diagonal $\mathbf{B}$ matrix can develop correlations throughout an assimilation window. Including correlations in $\mathbf{B}$ has been shown to significantly improve data assimilation results in numerical weather prediction [Bannister, 2008].

Including correlations between observation errors has only started to be explored recently in numerical weather prediction, with $\mathbf{R}$ still often treated as diagonal [Stewart et al., 2013]. Including some correlation structure in $\mathbf{R}$ has been shown to improve forecast accuracy [Weston et al., 2014]. Currently the correlations included in $\mathbf{R}$ have been mainly between observations made at the the same time rather than correlations between observations throughout time. When assimilating observations, data streams with many more observations can have a greater impact on the assimilation than those with fewer observations. In Richardson et al. [2010] this problem is discussed when assimilating large numbers of NEE observations along with smaller numbers of leaf area index and soil respiration observations. To address this problem Richardson uses a cost function that calculates the product of the departures from the ob-

servations rather than a cost function which sums these departures, giving a relative rather than absolute measure of the goodness-of-fit to the observations. Specifying serial correlations between observations represents another way of addressing this problem, whilst also adding valuable information to the data assimilation routine. Including serial correlations between observations of the same quantity decreases the impact of these observations [Järvinen et al., 1999] increasing the impact of less frequent observations.

In this paper we implement the new version of DALEC (DALEC2 [Bloom and Williams, 2015]) in a 4DVAR data assimilation scheme for joint state and parameter estimation, assimilating daily NEE observations from the Alice Holt flux site in Hampshire, UK which is managed by Forest Research [Wilkinson et al., 2012]. This assimilation scheme is then subjected to rigorous testing to ensure correctness. We then outline a new method for including parameter and state correlations in the background error covariance matrix and a method for including serial correlations in the observation error covariance matrix. These matrices are then used in a series of experiments in order to examine the effect that including correlations in the assimilation scheme has on the results. We show that specifying parameter and state correlations in the prior knowledge and serial correlations between observation errors can significantly improve the predicted carbon balance.

2 Model and Data Assimilation Methods

2.1 Alice Holt research forest

Alice Holt is an established research forest located in Hampshire, England with observational data spanning 50 years. The site is managed by Forest Research. The flux tower site is situated in the Straits Inclosure which is a mainly deciduous part of the forest comprising of mostly oak trees with a hazel understory, although there is a bank of conifer approximately 1km north west of the flux tower site [Pitman and Broadmeadow, 2001]. Flux tower records of Net Ecosystem Exchange (NEE) are available from 1999 up to present day [Wilkinson et al., 2012], meaning that Alice Holt has one of the longest records of flux tower NEE data in the world.

2.2 The DALEC2 model

The DALEC2 model is a simple process-based model describing the carbon balance of a forest ecosystem [Bloom and Williams, 2015] and is the new version of the original DALEC [Williams et al., 2005]. The model is constructed of six carbon pools (labile (C_{lab}), foliage (C_f), fine roots (C_r), woody stems and coarse roots (C_w), fresh leaf and fine root litter (C_l) and soil organic matter and coarse woody debris (C_s)) linked via fluxes. The aggregated canopy model (ACM) [Williams et al., 1997] is used to calculate daily gross primary production (GPP) of the forest, taking meteorological driving data and the modelled leaf area index (a function of C_f) as arguments. Figure 1 shows a schematic of how the carbon pools are linked in DALEC2.

The model equations for the carbon pools at day $t+1$ are as follows:

$$GPP^t = ACM(C_f^t, c_{lma}, c_{eff}, \Psi) \tag{1}$$

$$C_{lab}^{t+1} = (1-\Phi_{on})C_{lab}^t + (1-f_{auto})(1-f_{fol})f_{lab}GPP^t, \tag{2}$$

$$C_f^{t+1} = (1-\Phi_{off})C_f^t + \Phi_{on}C_{lab}^t + (1-f_{auto})f_{fol}GPP^t, \tag{3}$$

$$C_r^{t+1} = (1-\theta_{roo})C_r^t + (1-f_{auto})(1-f_{fol})(1-f_{lab})f_{roo}GPP^t, \tag{4}$$

$$C_w^{t+1} = (1-\theta_{woo})C_w^t + (1-f_{auto})(1-f_{fol})(1-f_{lab})(1-f_{roo})GPP^t, \tag{5}$$

$$C_l^{t+1} = (1-(\theta_{lit}+\theta_{min})e^{\Theta T^t})C_l^t + \theta_{roo}C_r^t + \Phi_{off}C_f^t, \tag{6}$$

$$C_s^{t+1} = (1-\theta_{som}e^{\Theta T^t})C_s^t + \theta_{woo}C_w^t + \theta_{min}e^{\Theta T^t}C_l^t, \tag{7}$$

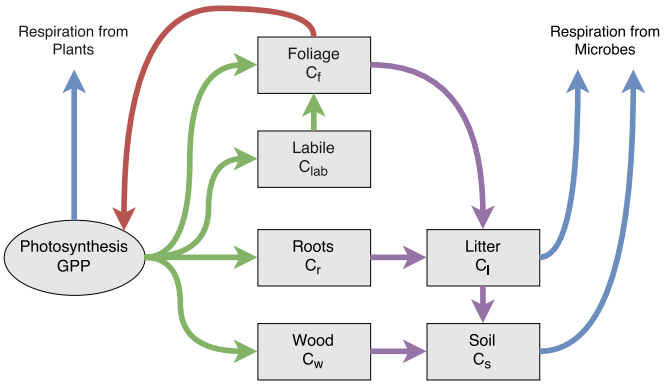

Figure 1: Representation of the fluxes in the DALEC2 carbon balance model. Green arrows represent C allocation, purple arrows represent litter fall and decomposition fluxes, blue arrows represent respiration fluxes and the red arrow represents the influence of leaf area index in the GPP function.

where T^t is the daily mean temperature, Ψ represents the meteorological driving data used in the GPP function and Φ_{on}/Φ_{off} are functions controlling leaf-on and leaf-off. The model parameters used in equations 1 to 7 are included in the appendix in table 4. DALEC2 differs from the original DALEC in that it can be parameterised for both deciduous and evergreen sites with Φ_{on} and Φ_{off} being able to reproduce the phenology of either type of site. The full details of this version of DALEC can be found in Bloom and Williams [2015].

2.3 4D-Var

In 4D-Var we aim to maximise the probability of $P(\mathbf{x}_0|\mathbf{y})$, the initial state $\mathbf{x}_0$ given a set of observations $\mathbf{y}$ over some time window, $0, \ldots, N$. The probability $P(\mathbf{x}_0|\mathbf{y})$ is maximised by minimising a cost function $J(\mathbf{x}_0)$ derived from Bayes Theorem [Lawless et al., 2013]. The cost function is given as,

$$J(\mathbf{x}_0) = \frac{1}{2}(\mathbf{x}_0 - \mathbf{x}_b)^T\mathbf{B}^{-1}(\mathbf{x}_0 - \mathbf{x}_b) + \frac{1}{2}\sum_{i=0}^{N}(\mathbf{y}_i - h_i(\mathbf{x}_i))^T\mathbf{R}_i^{-1}(\mathbf{y}_i - h_i(\mathbf{x}_i)), \tag{8}$$

where $\mathbf{x}_b$ is the so-called background and acts as the initial guess to the state $\mathbf{x}_0$, $\mathbf{B}$ is the background error covariance matrix and quantifies our knowledge of the error in the background, h_i is the observation operator at time t_i and maps the state vector evolved by the nonlinear model ($m_{0\rightarrow i}(\mathbf{x}_0) = \mathbf{x}_i$) to the observations at this time ($\mathbf{y}_i$) and $\mathbf{R}_i$ is the observation error covariance matrix at time t_i and represents our knowledge of the uncertainty in the observations. The state that minimises the cost function is called the analysis and is denoted as $\mathbf{x}_a$. This state is found using a minimisation routine that takes as its input arguments the cost function, the initial guess ($\mathbf{x}_b$) and also the gradient of the cost function given as,

$$\nabla J(\mathbf{x}_0) = \mathbf{B}^{-1}(\mathbf{x}_0 - \mathbf{x}_b) - \sum_{i=0}^{N}\mathbf{M}_{i,0}^T\mathbf{H}_i^T\mathbf{R}_i^{-1}(\mathbf{y}_i - h_i(\mathbf{x}_i)), \tag{9}$$

where $\mathbf{H}_i = \frac{\partial h_i(\mathbf{x}_i)}{\partial \mathbf{x}_i}$ is our linearized observation operator and $\mathbf{M}_{i,0} = \mathbf{M}_{i-1}\mathbf{M}_{i-2}\cdots\mathbf{M}_0$ is the tangent linear model with $\mathbf{M}_i = \frac{\partial m_i(\mathbf{x}_i)}{\partial \mathbf{x}_i}$. In practice $\nabla J(\mathbf{x}_0)$ is calculated using Lagrange multipliers as shown in Lawless et al. [2013]. We can rewrite the cost function and its gradient to avoid the sum notation as,

$$J(\mathbf{x}_0) = \frac{1}{2}(\mathbf{x}_0 - \mathbf{x}_b)^T\mathbf{B}^{-1}(\mathbf{x}_0 - \mathbf{x}_b) + \frac{1}{2}(\hat{\mathbf{y}} - \hat{h}(\mathbf{x}_0))^T\hat{\mathbf{R}}^{-1}(\hat{\mathbf{y}} - \hat{h}(\mathbf{x}_0)) \tag{10}$$

and

$$\nabla J(\mathbf{x}_0) = \mathbf{B}^{-1}(\mathbf{x}_0 - \mathbf{x}_b) - \hat{\mathbf{H}}^T\hat{\mathbf{R}}^{-1}(\hat{\mathbf{y}} - \hat{h}(\mathbf{x}_0)), \tag{11}$$

where,

$$\hat{\mathbf{y}} = \begin{pmatrix} \mathbf{y}_0 \\ \mathbf{y}_1 \\ \vdots \\ \mathbf{y}_N \end{pmatrix}, \; \hat{h}(\mathbf{x}_0) = \begin{pmatrix} h_0(\mathbf{x}_0) \\ h_1(m_{0\to 1}(\mathbf{x}_0)) \\ \vdots \\ h_N(m_{0\to N}(\mathbf{x}_0)) \end{pmatrix}, \; \hat{\mathbf{R}} = \begin{pmatrix} \mathbf{R}_{0,0} & \mathbf{R}_{0,1} & \dots & \mathbf{R}_{0,N} \\ \mathbf{R}_{1,0} & \mathbf{R}_{1,1} & \dots & \mathbf{R}_{1,N} \\ \vdots & \vdots & \ddots & \vdots \\ \mathbf{R}_{N,0} & \mathbf{R}_{N,1} & \dots & \mathbf{R}_{N,N} \end{pmatrix} \text{ and } \; \hat{\mathbf{H}} = \begin{pmatrix} \mathbf{H}_0 \\ \mathbf{H}_1\mathbf{M}_0 \\ \vdots \\ \mathbf{H}_N\mathbf{M}_{N,0} \end{pmatrix}. \tag{12}$$

Solving the cost function in this form also allows us to build serial correlations into the observation error covariance matrix $\hat{\mathbf{R}}$. The off-diagonal blocks of $\hat{\mathbf{R}}$ represent correlations in time between assimilated observations and are usually taken to be zero.

2.4 Implementation and testing of 4D-Var system

In our DALEC2 4D-Var scheme we are performing joint parameter and state estimation. Therefore the state vector, $\mathbf{x}_0$, corresponds to the vector of the 17 model parameters and 6 initial carbon pool values, which can be found in the appendix. Here the nonlinear model (DALEC2) only updates the initial carbon pool values when evolving the state vector forward in time with the parameters being held constant. To find the background guess, $\mathbf{x}_b$, to the state vector we can either use a previous DALEC2 model forecast's estimate to the state of the system for the site (when available) or use expert elicitation to define likely state and parameter values and ranges for the site. The background vector ($\mathbf{x}_b$) and its corresponding standard deviations (see table 4) used in this paper were provided from existing runs of the the CARbon DAta-MOdel fraMework (CARDAMOM) [Exbrayat et al., 2015]. This is a worse resolution dataset which provides a reasonable first guess at DALEC2 state and parameter values for the Alice Holt research site.

In order to find the tangent linear model (TLM) for DALEC2 it is necessary to find the derivative of the model at each time step with respect to the 17 model parameters and the 6 carbon pools. We use the AlgoPy automatic differentiation package [Walter and Lehmann, 2013] in Python to calculate the TLM at each time step. This package uses forward mode automatic differentiation to calculate the derivative of our model. In the following tests we use a diagonal approximation to our background and observational error covariance matrices so that, $\mathbf{B}_{diag} = \text{diag}(\boldsymbol{\sigma}_b)^2$ and $\hat{\mathbf{R}}_{diag} = \text{diag}(\boldsymbol{\sigma}_o)^2$, where $\boldsymbol{\sigma}_b$ and $\boldsymbol{\sigma}_o$ are the vectors of the background and observational standard deviations respectively.

In this paper we assimilate observations of daily NEE. The flux tower actually produces an estimate of NEE every half-hour. We take the sum over the 48 measurements made each day. We only select days where there is no missing data and over 90% of observations have a quality control flag associated with the best observations from the EddyPro flux processing software [LI-COR, Inc., 2015]. We take a variance of $0.5\text{gCm}^{-2}\text{day}^{-1}$ in our assimilated observations of daily NEE [Williams et al., 2005]. The minimisation routine used in our data assimilation experiments is the truncated Newton method [Nocedal and Wright, 1999] from the Python package Scipy.optimize. In sections 2.4.1 to 2.4.3 we show tests of our scheme.

2.4.1 Test of tangent linear model

We can have confidence that our implementation of the TLM for DALEC2 is correct as it passes the following relevant tests [Li et al., 1994]. In 4D-Var we assume the tangent linear hypothesis,

$$m_{0\to i}(\mathbf{x}_0 + \gamma\delta\mathbf{x}_0) \approx m_{0\to i}(\mathbf{x}_0) + \mathbf{M}_{i,0}\gamma\delta\mathbf{x}_0, \tag{13}$$

where $\delta\mathbf{x}_0$ is a perturbation of the initial state and γ is a parameter controlling the size of this perturbation.The validity of this assumption depends on how nonlinear the model is, the length of the assimilation window and the size of the perturbation $\delta\mathbf{x}_0$. We can test this by rearranging equation 13 to find the relative error,

$$E_R = \frac{||m_{0\to i}(\mathbf{x}_0 + \gamma\delta\mathbf{x}_0) - m_{0\to i}(\mathbf{x}_0)||}{||\mathbf{M}_{i,0}\gamma\delta\mathbf{x}_0||}, \tag{14}$$

where we expect $E_R \to 0$ as $\gamma \to 0$ (here we are using the Euclidean norm). Figure 2 shows equation 14 plotted for DALEC2 with a TLM evolving our state 731 days forward in time for different values γ, with a 5% perturbation $\delta\mathbf{x}_0$. Figure 2 shows that the TLM behaves as expected for values of γ approaching 0.

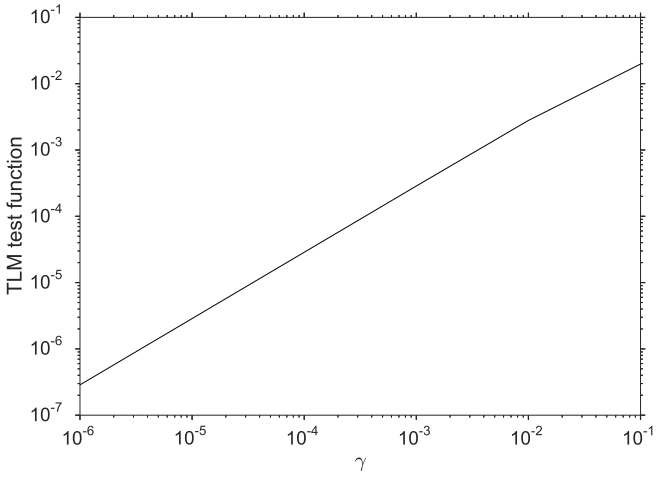

Figure 2: Plot of the tangent linear model test function (equation 14) for DALEC2, for a TLM evolving our state 731 days forward in time and a 5% perturbation, $\delta\mathbf{x}_0$.

It is also useful to show how our TLM behaves over a time window to see how the error in the TLM grows as we evolve our state further forward in time. We again rearrange equation 13 with an additional error term to find,

$$\text{percentage error in TLM} = \left| \frac{||m_{0\to i}(\mathbf{x}_0+\delta\mathbf{x}_0) - m_{0\to i}(\mathbf{x}_0)||}{||\mathbf{M}_{i,0}\delta\mathbf{x}_0||} - 1 \right| \times 100. \tag{15}$$

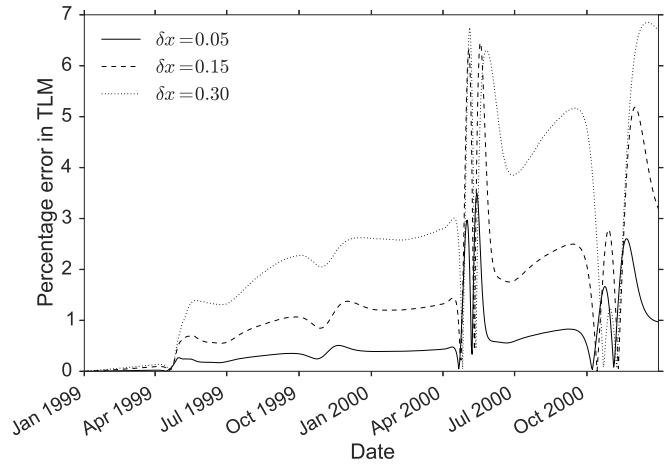

Figure 3: Plot of the percentage error in the tangent linear model (equation 15) for DALEC2 when evolving the model state forward over a period of two years with three differing values of perturbation, $\delta\mathbf{x}_0$.

In figure 3 we can see that our TLM for DALEC2 performs well after being run forward a year with less than a 3% error for all values of $\delta\mathbf{x}_0$. By the second year we see some peaks in our error in spring and autumn. This is due to leaf on and leaf off functions in the TLM going out of phase with the nonlinear DALEC2. Even at these peaks our error is still reasonable reaching a maximum at 7% and then coming back to around 1%. For this reason we present results using a one year assimilation window in this paper.

2.4.2 Test of adjoint model

The adjoint model we have implemented for DALEC2 passes correctness tests. For our TLM $\mathbf{M}_{i,0}$ and its adjoint $\mathbf{M}_{i,0}^T$ we have the identity

$$< \mathbf{M}_{i,0}\delta\mathbf{x}_0, \mathbf{M}_{i,0}\delta\mathbf{x}_0 >=< \delta\mathbf{x}_0, \mathbf{M}_{i,0}^T\mathbf{M}_{i,0}\delta\mathbf{x}_0 > \tag{16}$$

for any inner product $<,>$ and perturbation $\delta\mathbf{x}_0$, this is derived from the adjoint identity [Lawless et al., 2013]. Using the Euclidean inner product equation 16 is equivalent to

$$(\mathbf{M}_{i,0}\delta\mathbf{x}_0)^T(\mathbf{M}_{i,0}\delta\mathbf{x}_0) = \delta\mathbf{x}_0^T(\mathbf{M}_{i,0}^T(\mathbf{M}_{i,0}\delta\mathbf{x}_0)). \tag{17}$$

We evaluated the left hand side and right hand side of this identity for differing values of $\delta\mathbf{x}_0$ and showed that they were equal to machine precision.

2.4.3 Gradient test

The 4D-Var system we have developed passes tests for the gradient of the cost function [Navon et al., 1992]. In the implementation of the cost function and its gradient we regularise the problem using a variable transform [Freitag et al., 2010]. For our cost function J and its gradient ∇J we can show that we have implemented ∇J correctly using the identity,

$$f(\alpha) = \frac{|J(\mathbf{x}_0 + \alpha\mathbf{b}) - J(\mathbf{x}_0)|}{\alpha\mathbf{b}^T\nabla J(\mathbf{x}_0)} = 1 + O(\alpha), \tag{18}$$

where $\mathbf{b}$ is a vector of unit length and α is a parameter controlling the size of $\mathbf{b}$. For small values of α not too close to machine precision we should have $f(\alpha)$ close to 1. Figure 4a shows $f(\alpha)$ for a 365 day assimilation window with $\mathbf{b} = \mathbf{x}_0||\mathbf{x}_0||^{-1}$, we can see that $f(\alpha) \to 1$ as $\alpha \to 0$, as expected until $f(\alpha)$ gets too close to machine zero at $O(\alpha) = 10^{-11}$.

We can also plot $|f(\alpha) - 1|$, where we expect $|f(\alpha) - 1| \to 0$ as $\alpha \to 0$. In figure 4b we have plotted $|f(\alpha) - 1|$ for the same conditions as in figure 4a, we can see that $|f(\alpha) - 1| \to 0$ as $\alpha \to 0$, as expected (before $|f(\alpha) - 1|$ gets too close to machine precision at $O(\alpha) = 10^{-8}$). This gives us confidence that the gradient of our cost function is implemented correctly.

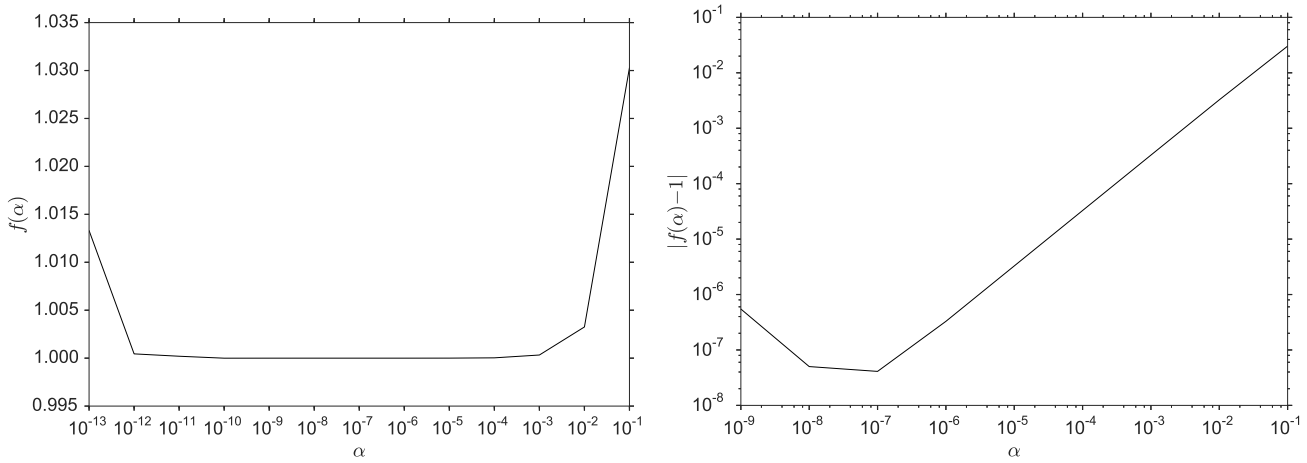

(a) $f(\alpha)$ test

(b) $|f(\alpha) - 1|$ test

Figure 4: Tests of the gradient of the cost function for a 365 day assimilation window with $\mathbf{h} = \mathbf{x}_0||\mathbf{x}_0||^{-1}$.

2.5 Including correlations in the background error covariance matrix

As discussed in section 1, including correlations in $\mathbf{B}$ impacts how information from assimilated observations is spread between different types of analysis variables [Bannister, 2008]. We explored a number of different methods in order to include parameter-state correlations in $\mathbf{B}$. In this paper we present a method using a set of ecological dynamical constraints on model parameters and state variables from Bloom and Williams [2015]. In Bloom and Williams [2015] implementing these constraints in a Metropolis Hastings MCMC data assimilation routine is shown to improve results significantly. The constraints impose conditions on carbon pool turnover and allocation ratios, steady state proximity and growth and decay of model carbon pools.

In order to create a correlated background error covariance matrix, $\mathbf{B}_{corr}$, using these constraints we create an ensemble of state vectors which we then take the covariance of to give us $\mathbf{B}_{corr}$. To create this ensemble we use the following procedure:

1. Draw a random state vector, $\mathbf{x}_i$, from the multivariate truncated normal distribution described by our $\mathbf{x}_b$, associated variances and parameter-state ranges given in table 4.

2. Test this $\mathbf{x}_i$ with the ecological dynamical constraints (requiring us to run the DALEC2 model using this state).

3. If $\mathbf{x}_i$ passes it is added to to our ensemble, else it is discarded.

Once we have a full ensemble (we chose an ensemble size of 1500 as past this point values of correlations did not appear to change significantly) we then take the covariance of the ensemble to find $\mathbf{B}_{corr}$. In figure 5 we have plotted the correlation matrix or normalised error covariance matrix of $\mathbf{B}_{corr}$. This matrix includes both positive and negative correlations between parameter and state variables, with correlations of 1 down the diagonal between variables of the same quantity as expected. The largest positive off-diagonal correlation being 0.42 between f_{lab} and C_{lab}. This makes physical sense as f_{lab} is the parameter controlling the amount of GPP allocated to the labile carbon pool, C_{lab}.

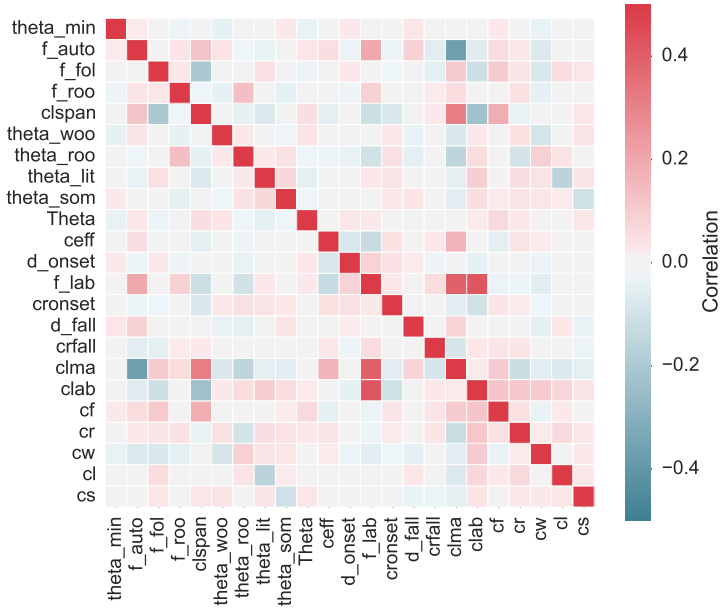

Figure 5: Background error correlation matrix created using method in section 2.5

2.6 Specifying serial correlations in the observational error covariance matrix

Errors in NEE observations come from different sources such as instrument errors, sampled ecosystem structure and turbulent conditions (when we have low turbulence and limited air mixing NEE is underestimated) [Papale et al., 2006]. Due to this dependance on atmospheric conditions we expect the errors in observations of NEE to be serially correlated, as the atmospheric signal itself is serially correlated [Daley, 1992]. If we were assimilating half hourly observations of NEE we would expect stronger correlations between observation errors, as atmospheric conditions are more constant at this time scale, with correlations between observation errors getting weaker with lower frequency observations. The observation error covariance matrix does not only represent the instrumentation error for an observation but also the error in the observation operator (mapping the model state to the observation) and representativity error (error arising from the model being unable resolve the spatial and temporal scales of the observations). These other sources of error represented in $\hat{\mathbf{R}}$ can also lead to correlations between observation errors [Waller et al., 2014].

In section 2.3 we have re-written the 4D-Var cost function in equation 10 in order to allow the specification of serial observation error correlations in our assimilation scheme. These serial correlations are represented by the off-diagonal blocks of $\hat{\mathbf{R}}$. In work carried out with spatial correlations it has been shown that the structure of the correlation is not critical [Healy and White, 2005] and that it is better to include some estimate of error correlation structure in the observation error covariance matrix than wrongly assume that errors are independent [Stewart et al., 2013]. As a first attempt we try including correlations on the scale of the observation frequency. We adapt the simple Gaussian model found in Järvinen et al. [1999] (a second order autoregressive correlation function was also tested but not presented here). The correlation r between 2 observations at times t_1 and t_2 is given as,

$$r = \begin{cases} a\exp\left[\frac{-(t_1-t_2)^2}{\tau^2}\right] + (1-a)\delta_{t_1-t_2} & |t_1 - t_2| \leq \eta \\ 0 & \eta < |t_1 - t_2| \end{cases}, \tag{19}$$

where τ is the e-folding time, a controls the strength of correlation, δ is the Kronecker delta and η is the cut off time after which the correlation between two observation errors is zero. We have incorporated a cut off for correlations between observation errors as the assumed correlation length scale for our assimilated observations is short. This cut off along with the form of correlation function using the Kronecker delta helps ensure $\hat{\mathbf{R}}$ is positive definite and therefore invertible, as required in the assimilation process.

Figure 6 shows $\hat{\mathbf{R}}$ created using equation 19, there are 67 NEE observations in this one year assimilation window, these observations are not all on adjacent days and this is evident in the structure of $\hat{\mathbf{R}}$. The effect of the short e-folding time chosen here ($\tau = 4$) provides the desired structure.

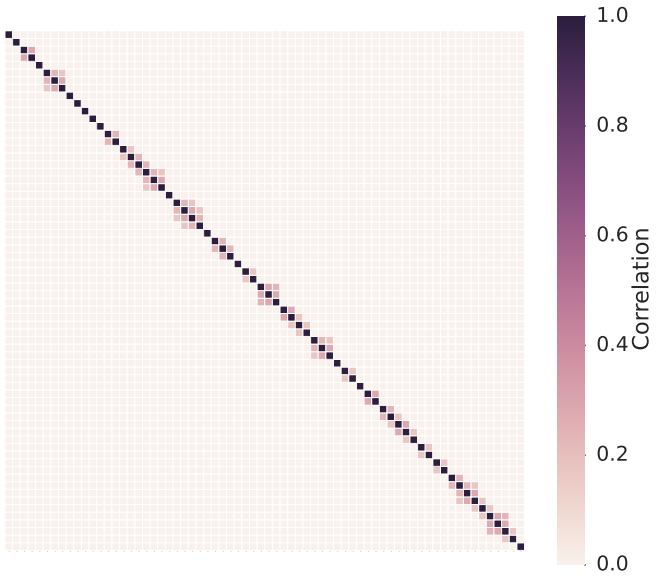

Figure 6: Observation error covariance matrix for the 67 observations used in assimilation created using method in section 2.6 with $\tau = 4$, $a = 0.3$ and $\eta = 4$.

3 Results

3.1 Experiments

In the following sections we present the results of 4 experiments where we vary the representations of $\mathbf{B}$ and $\hat{\mathbf{R}}$ while assimilating the same NEE observations in the window from 1999-2000. As shown in figure 3 the performance of the tangent linear model deteriorates after the first year. We then forecast the NEE over the next 14 years and compare with the observed data. These experiments are outlined in table 1 where $\mathbf{B}_{diag}$ and $\hat{\mathbf{R}}_{diag}$ are the diagonal matrices of the parameter-state variances and the observations variances respectively and $\mathbf{B}_{corr}$ and $\hat{\mathbf{R}}_{corr}$ are the matrices as specified in section 2.5 and section 2.6 respectively.

Experiment	$\mathbf{B}_{diag}$	$\hat{\mathbf{R}}_{diag}$	$\mathbf{B}_{corr}$	$\hat{\mathbf{R}}_{corr}$
A	×	×		
B		×	×	
C	×			×
D			×	×

Table 1: The combination of error covariance matrices used in each data assimilation experiment.

3.2 Experiment A

In this experiment $\mathbf{B}_{diag}$ and $\hat{\mathbf{R}}_{diag}$ were used in our assimilation as described in section 3.1. Because these contain no correlations this experiment forms the baseline by which the subsequent results from assimilation experiments are judged.

Figure 7a shows assimilation and forecast results for NEE. We can see that assimilating the observations of NEE has improved the background with our analysis trajectory (green line) fitting well with the observations during the the assimilation window (1999-2000). The analysis trajectory then diverges

in the forecast (2000-2014). This can be seen more clearly in figue 8a, where we have an over prediction of respiration in the winter and the seasonal cycle does not match the observations. As discussed in section 1 previous work has shown the importance of specifying parameter-state correlations when using variational data assimilation for joint parameter-state estimation [Smith et al., 2009]. Although in 4D-Var some correlation structure is added implicitly as $\mathbf{B}_{diag}$ is evolved through time, observations near the beginning of the window (before significant correlations develop in $\mathbf{B}_{diag}$) will not be spread in a multivariate way. The correlations developed by the implicit evolution of $\mathbf{B}_{diag}$ may also not include important physical relationships between variables. Therefore by not specifying these correlations in this experiment we allow our parameter and state variables to attain unrealistic values in order to find the best fit to the observations in the analysis window (1999-2000), leading to the divergence seen in the forecast (1999-2014).

To see how well our forecast performs after assimilation we show a scatter plot of modelled NEE against observed NEE in figure 9a. Here we have a Root-Mean-Square Error (RMSE) of 4.22gCm^{-2} and a bias of -0.3gCm^{-2} for our forecast of NEE, whereas our analysis (1999-2000) has a RMSE of 1.36gCm^{-2} and a bias of -0.03gCm^{-2}. The background trajectory meanwhile has a RMSE of 3.86gCm^{-2} and a bias of -1.60gCm^{-2} in the analysis window (1999-2000) and the same RMSE of 3.86gCm^{-2} but a bias of -1.36gCm^{-2} during the forecast period (2000-2014). Although using $\mathbf{B}_{diag}$ and $\hat{\mathbf{R}}_{diag}$ in our assimilation has considerably reduced the RMSE in our analysis period, it has also increased the RMSE in our forecast of NEE. However it has reduced the bias in the model forecast considerably from -1.36gCm^{-2} to -0.3gCm^{-2}. The bias in the background comes from a constant under prediction of the more extreme negative values of NEE and this leads to considerably worse results than our analysis and its forecast for total forest carbon uptake.

3.3 Experiment B

Here $\mathbf{B}_{corr}$ (as defined in section 2.5) and $\hat{\mathbf{R}}_{diag}$ are used in our assimilation. Figure 7b shows assimilation and forecast results for NEE. In figure 8b we can see that the forecast performs considerably better than in experiment A, with the analysis trajectory no longer over predicting winter respiration and matching the observed seasonal of NEE more closely in the forecast period (2000-2014). From figure 9b and table 3 we see that our forecasts RMSE has almost halved (now 2.56gCm^{-2}) with a reduction in bias also, now -0.2gCm^{-2}. In comparison using $\mathbf{B}_{corr}$ in our assimilation very slightly degrades the fit for our analysis (1999-2000), with a RMSE of 1.42gCm^{-2} and a bias of -0.04gCm^{-2}, as shown in table 2.

We can see the effect that including correlations in $\mathbf{B}$ has on the analysis update in figure 10. For some variables including correlations in $\mathbf{B}$ has had a large impact on the analysis update after assimilation. This is particularly clear for the f_{lab} parameter. The largest positive off-diagonal correlation in $\mathbf{B}_{edc}$ is between C_{lab} and f_{lab}, with f_{lab} also having a large positive correlation with c_{lma} as shown in section 2.5. The effect of these correlations has been to change the analysis increment for f_{lab} from being slightly positive in experiment A to being strongly negative by following the analysis update of its correlated variables C_{lab} and c_{lma}. The added constraint provided by the correlations in $\mathbf{B}_{edc}$ reduces the likelihood that parameter and state variables will attain unrealistic values in order to fit the assimilated observations. Although this has led to a slightly degraded fit to the observations in the analysis window (1999-2000) it has also significantly improved the fit to observations for the forecast (1999-2014).

3.4 Experiment C

Here we use $\mathbf{B}_{diag}$ and $\hat{\mathbf{R}}_{corr}$ (as defined in section 2.6) in the assimilation. Results shown in figure 7c and 8c appear similar to those in section 3.2 however there are some differences. From table 3 and figure 9c we see a slight reduction in RMSE for our forecast (now 4.09gCm^{-2}) in comparison with experiment A. As in experiment B the fit to the observations in the analysis window (1999-2000) is very slightly degraded as the added correlations in $\hat{\mathbf{R}}_{corr}$ act to reduce the weight of the observations in the

assimilation [Järvinen et al., 1999]. The changes seen when using $\hat{\mathbf{R}}_{corr}$ in the assimilation are less than when using $\mathbf{B}_{corr}$ as the correlations specified in $\hat{\mathbf{R}}_{corr}$ are on a short timescale and smaller than those in $\mathbf{B}_{corr}$, the background error covariance matrix also plays a larger role in the assimilation spreading information between parameter and state variables [Bannister, 2008]. In figure 10 we can see that the changes between experiment A and C in the analysis increment are much less than when using $\mathbf{B}_{edc}$.

We also expect that specifying correlations in $\hat{\mathbf{R}}$ will help when assimilating other less frequently sampled data streams along with NEE as the serial correlations reduce the weight given to the mean of the observations and also reduce the information content of the data streams with more observations [Daley, 1992, Järvinen et al., 1999].

3.5 Experiment D

In the final experiment we use $\mathbf{B}_{corr}$ and $\hat{\mathbf{R}}_{corr}$ in the assimilation. Figure 7d and figure 7d shows that using both correlated matrices gives similar results as experiment B when $\mathbf{B}_{corr}$ is used with $\hat{\mathbf{R}}_{diag}$. However using $\hat{\mathbf{R}}_{corr}$ in addition to $\mathbf{B}_{corr}$ provides similar improvements as in experiment C. From table 3 and figure 9d we see the forecast RMSE is reduced again still from results in experiment B to 2.38gCm^{-2}. Using both matrices appears to combine the beneficial effects described in both section 3.3 and section 3.4. In figure 10 we can see that the analysis increment is very similar to experiment B.

3.6 Summary

In our experiments we have shown that both $\mathbf{B}_{corr}$ and $\hat{\mathbf{R}}_{diag}$ have the effect of improving the model forecast of NEE. As it can be difficult to inspect the skill of a certain model by only plotting model trajectories, in figure 11 we show Taylor diagrams displaying a statistical comparison of the four experiment and background analysis (1999-2000) and forecast (2000-2014) results with the observations of NEE. Here the radial distances from the origin to the points are proportional to the pattern standard deviations and the azimuthal positions give the correlation coefficient between the modelled and observed NEE [Taylor, 2001]. If a model predicted the observations perfectly it would have a correlation coefficient of 1 and a radial distance matching that of the observations (represented by the dotted line). Figure 11a shows that all the experiments give very similar results in the analysis window (1999-2000) with all the experiment points closely grouped on top of each other. Whereas figure 11b shows the significant difference between the experiment results in the forecast (2000-2014).

Experiment	RMSE (gCm^{-2})	Bias (gCm^{-2})	Correlation coefficient
Background	3.86	−1.60	0.70
A	1.36	−0.03	0.96
B	1.42	−0.04	0.95
C	1.37	−0.09	0.96
D	1.43	−0.09	0.95

Table 2: Analysis (1999-2000) results for experiments and background when judged against observed NEE.

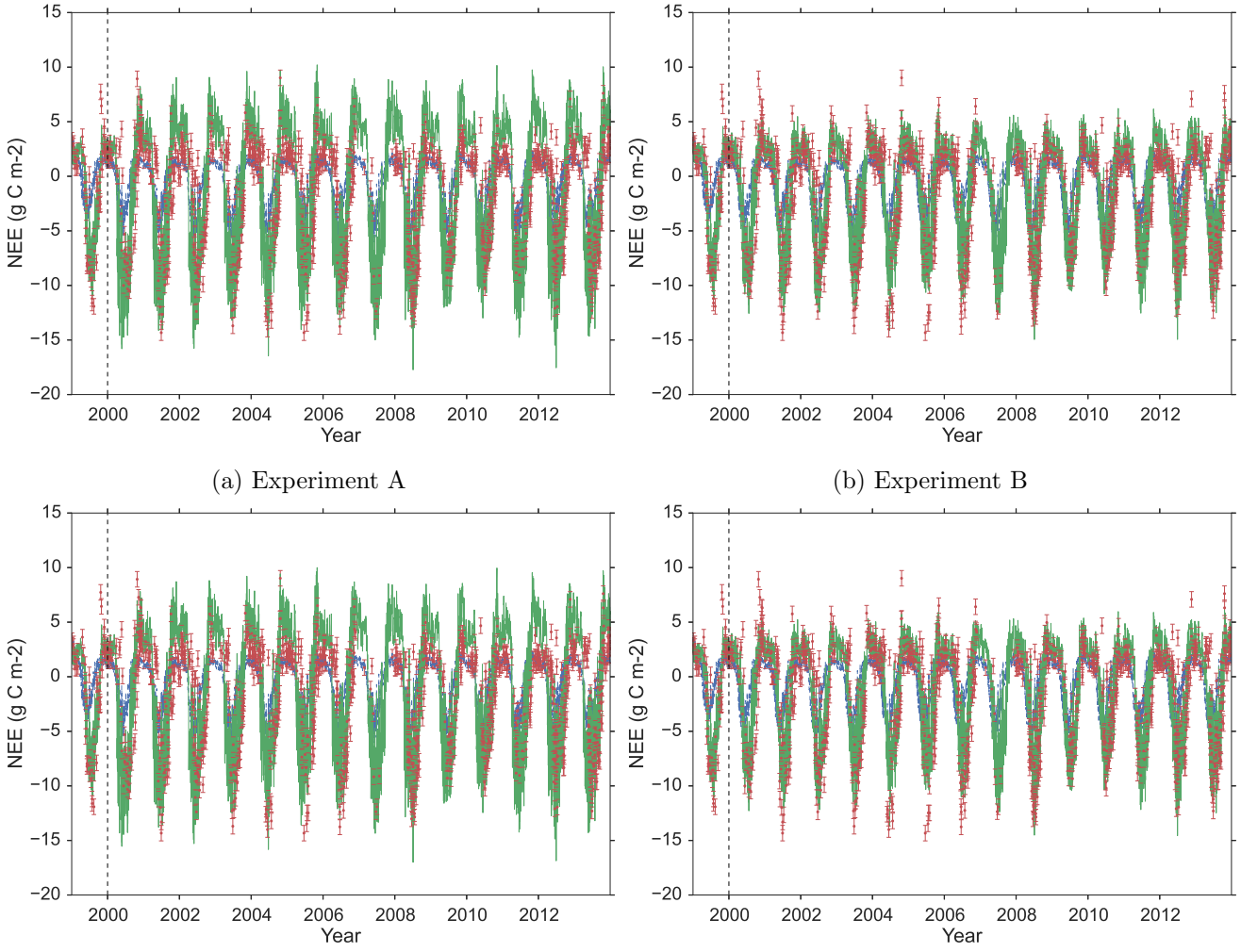

(a) Experiment A

(b) Experiment B

(c) Experiment C

(d) Experiment D

Figure 7: One year assimilation and fourteen year forecast of Alice Holt NEE with DALEC2, blue dotted line: background model trajectory, green line: analysis and forecast after assimilation, red dots: observations from Alice Holt flux site with error bars.

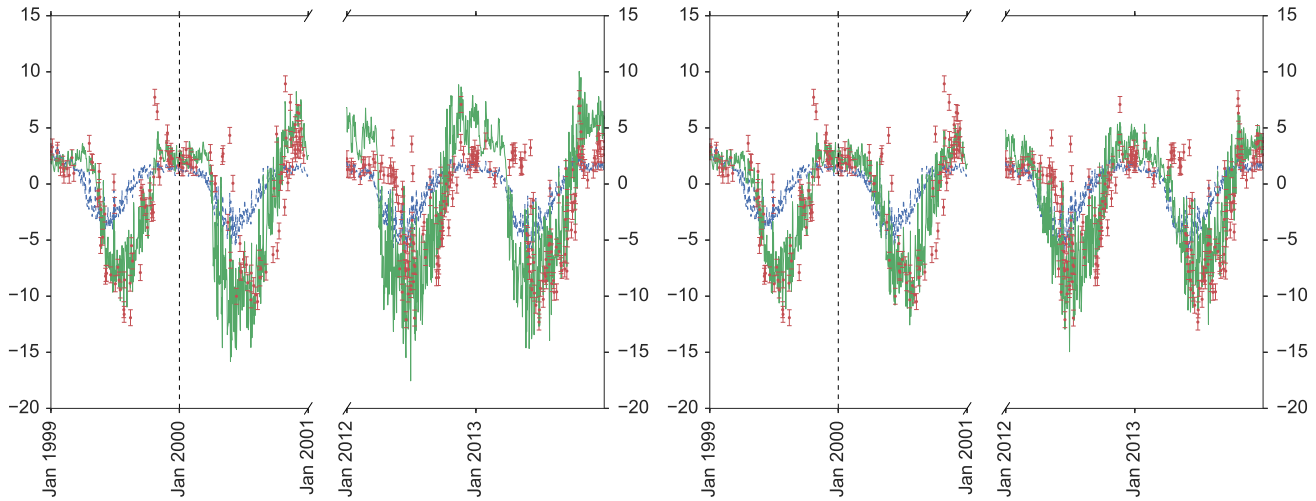

(a) Experiment A

(b) Experiment B

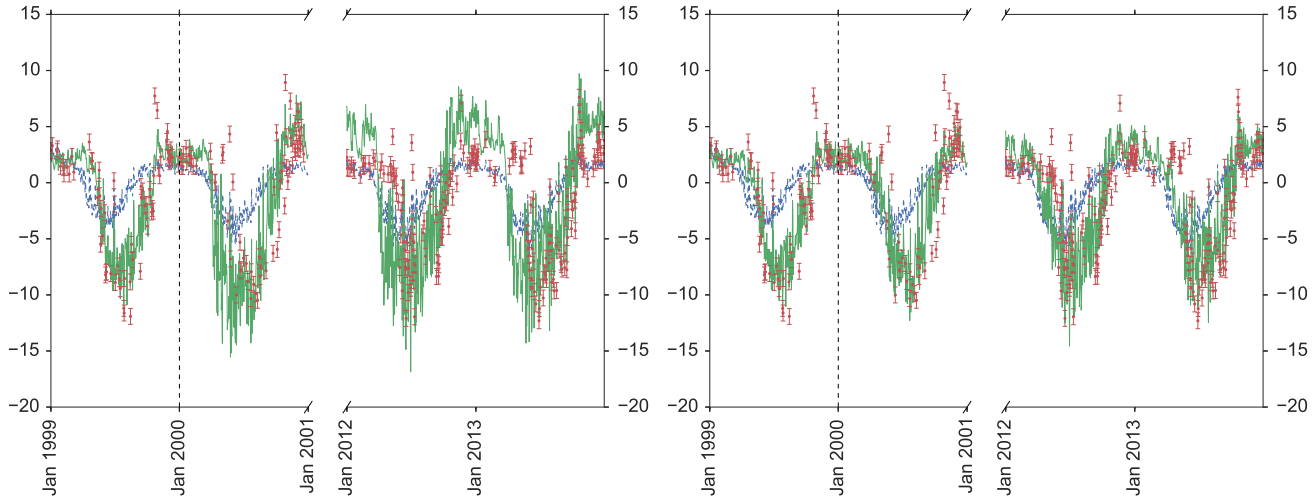

(c) Experiment C

(d) Experiment D

Figure 8: Broken plot showing the first and final two years results from the one year assimilation and fourteen year forecast of Alice Holt NEE with DALEC2, blue dotted line: background model trajectory, green line: analysis and forecast after assimilation, red dots: observations from Alice Holt flux site with error bars.

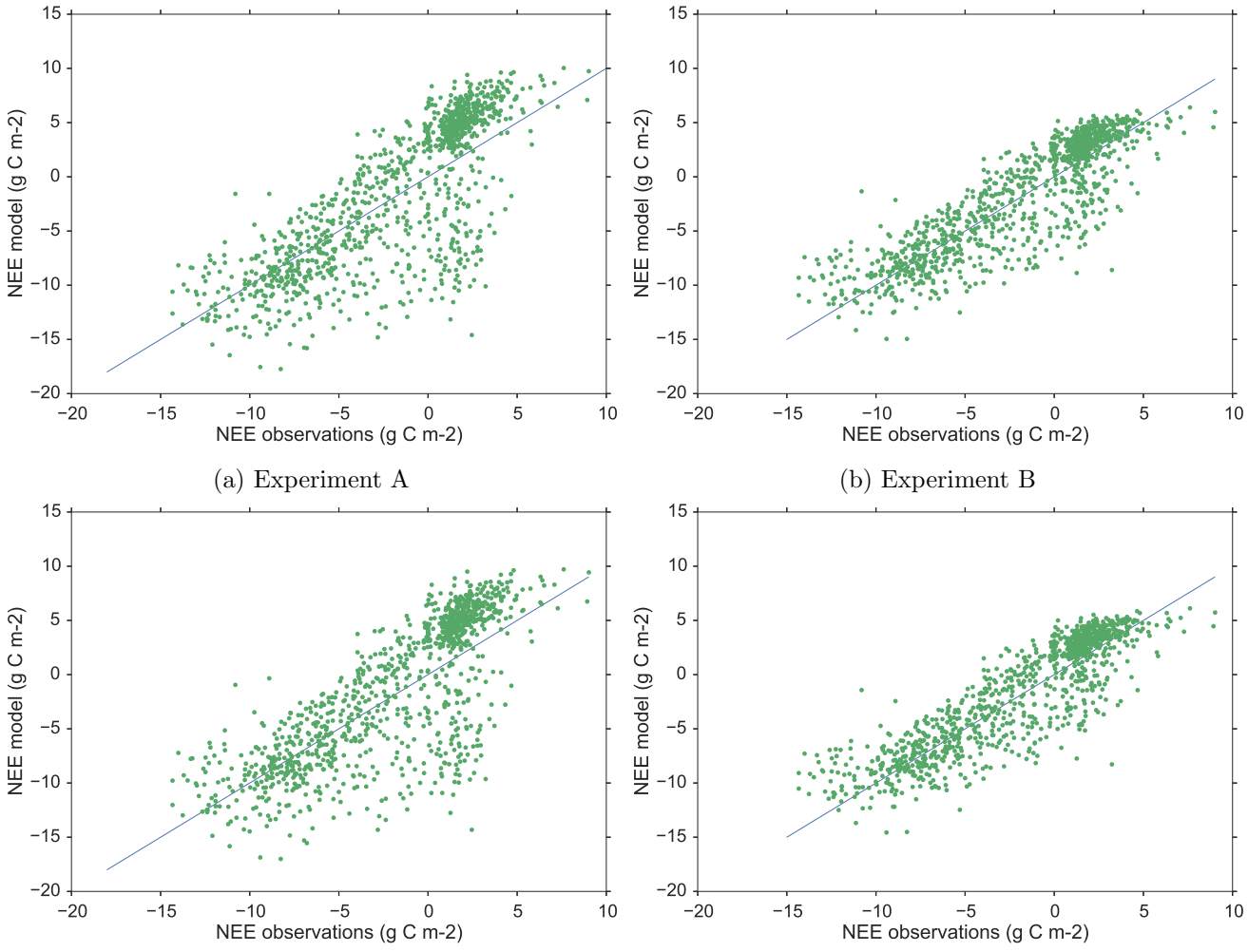

(a) Experiment A

(b) Experiment B

(c) Experiment C

(d) Experiment D

Figure 9: Forecast scatter plot of modelled NEE vs. observations for 2000-2014 (green dots). Blue line represents the 1-1 line.

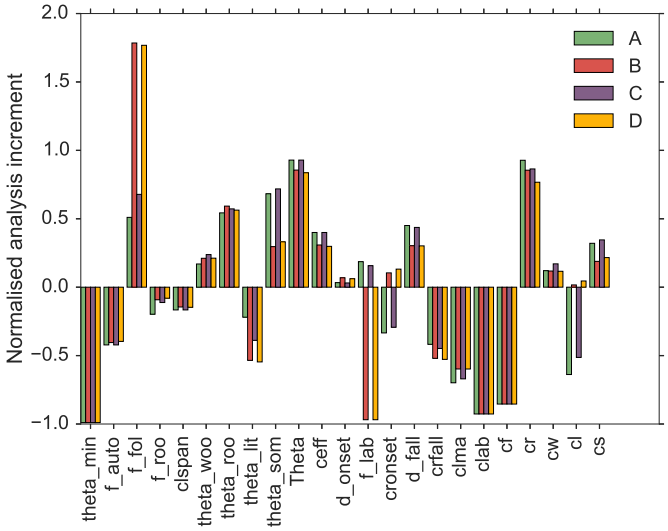

Figure 10: Normalised analysis increment for the four experiments.

Experiment	RMSE (gCm^{-2})	Bias (gCm^{-2})	Correlation coefficient
Background	3.86	−1.36	0.66
A	4.22	−0.30	0.79
B	2.56	−0.20	0.87
C	4.09	−0.51	0.78
D	2.38	−0.33	0.88

Table 3: Forecast (2000-2014) results for experiments and background when judged against observed NEE.

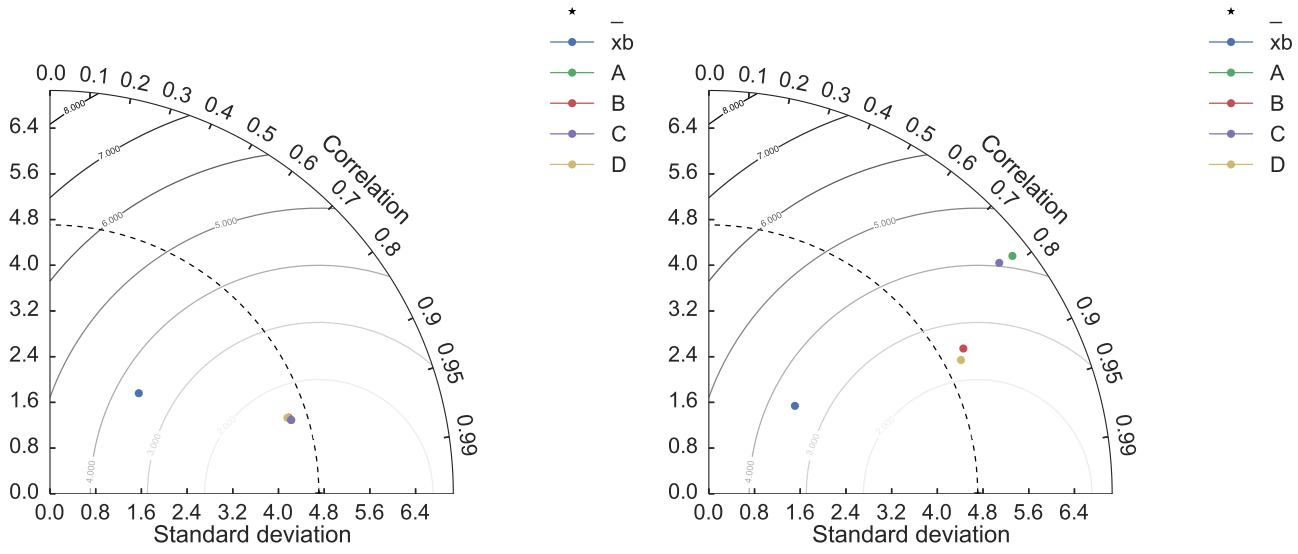

(a) Analysis (1999-2000)

(b) Forecast (2000-2014)

Figure 11: Taylor diagrams displaying statistical comparison of the four experiment and background analysis (1999-2000) and forecast (2000-2014) results with observations of NEE (gCm^{-2}). The dotted line represents the standard deviation of the observations and the contours represent values of constant root mean square error between model and observations.

4 Discussion

In this paper we have implemented the DALEC2 functional ecology model in a 4D-Var data assimilation scheme, building an adjoint of the DALEC2 model and applying rigorous tests to our scheme. Using 4D-Var can provide much faster assimilation results than MCMC techniques as we have knowledge of the derivative of the model. For our experiments the 4D-Var routine has taken $O(10^2)$ function evaluations to converge to a minimum, whereas MCMC techniques using the same model take $O(10^8)$ function evaluations [Bloom and Williams, 2015]. However we do also assume that the problem is Gaussian whereas MCMC techniques do not. We have shown that 4D-Var is a valid tool for improving the DALEC2 model estimate of NEE and that even when assimilating a single year of NEE observations we can improve our forecast significantly. In practice this type of data assimilation routine would be run in cycling mode running the analysis from the first year as the background for the second then iterating this until all data is assimilated.

We then considered the nature of background and observational errors. The effect of specifying parameter-state correlations in our background information and serial correlations between our observation errors was explored.

The technique presented here to specify $\mathbf{B}_{corr}$ has been shown to significantly improve forecasts of NEE over using a diagonal representation of $\mathbf{B}$. These results agree with those of Smith et al. [2009] where the importance of specifying parameter-state correlations when performing joint parameter-state estimation with variational data assimilation is shown. The method for specifying $\mathbf{B}_{corr}$ in this paper used a series of ecological dynamical constraints taken from Bloom and Williams [2015]. In cases where these type of constraints are not available there are other methods to build correlations into $\mathbf{B}$. One technique we also tested (not presented here) to create a correlated $\mathbf{B}$ involved evolving an ensemble of state vectors over the length of the chosen assimilation window using the model (DALEC2) and then taking the covariance of the evolved ensemble. This gave us a $\mathbf{B}$ with parameter-state and state-state correlations, but no parameter-parameter correlations as the parameters are not updated by the model. Using the $\mathbf{B}$ created with this method also improved assimilation results significantly over using a diagonal $\mathbf{B}$. Many different tests were run using different background vectors and variances and it was found that specifying some form of correlation structure in $\mathbf{B}$ always made some improvement to the results of our assimilation.

In NWP it has been shown that including correlations in $\mathbf{R}$ can help improve data assimilation results [Weston et al., 2014]. However the specified correlations have most commonly been spatial correlations with observations errors still being considered independent in time. In this paper we have shown that including correlations between observation errors in time can also improve data assimilation results, here improving the DALEC2 model forecast of NEE. We expect including these serial correlations to have an even greater impact when assimilating more than one data stream. When assimilating multiple data streams more frequently sampled observation types (such as NEE) have much more impact on the assimilation than data streams sampled less frequently. Specifying serial correlations between observations of the same type has the effect of reducing the weight given to the mean of the observations [Järvinen et al., 1999], thus allowing less frequent data streams to have more impact on the assimilation. Using the form of $\hat{\mathbf{R}}$ given in this paper for specifying serial correlations will also allow us to specify serial correlations between different observation types. When running the model with a day-night time step this will allow us to build in the type of correlations investigated by Baldocchi et al. [2015] between ecosystem respiration and canopy photosynthesis.

The $\hat{\mathbf{R}}_{corr}$ present in this paper has a weak correlation ($a = 0.3$) between observations of NEE in time, this representation of $\hat{\mathbf{R}}_{corr}$ has improved the model forecast of NEE. However other choices of $\hat{\mathbf{R}}_{corr}$ (with stronger correlations between observations) tested for this paper degraded the forecast. This is probably due to the specified correlations being unrealistic and suggests a more diagnostic approach is needed for the calculation of serial correlations in $\hat{\mathbf{R}}$. One option would be to adapt the Desroziers et al. [2005] diagnostic, which has been used successfully in NWP for diagnosing observation error correlations

for observations taken at the same time, and extending this technique to diagnose serial correlations. This will form the basis of future work.

Including correlations in both $\mathbf{B}$ and $\mathbf{R}$ improve the DALEC2 model forecast of NEE significantly. From the results in experiment D (using both $\mathbf{B}_{corr}$ and $\hat{\mathbf{R}}_{corr}$) and integrating over the area of the Alice Holt flux site ($\sim 0.93\text{km}^2$) the forecasted (2000-2014) total carbon uptake for the Alice Holt research site is 5.04×10^9gC. In comparison the less accurate results from experiment A (using $\mathbf{B}_{diag}$ and $\hat{\mathbf{R}}_{diag}$) predict a total carbon uptake of 5.26×10^9gC, a difference of 2.25×10^8gC. This is quite a substantial difference as we are considering the carbon uptake of a small ($\sim 0.93\text{km}^2$) research site only. We plan on applying these techniques to other sites and also assimilating multiple data streams with varying sampling frequency to investigate the effect of including correlations in $\mathbf{B}$ and $\mathbf{R}$ further.

5 Conclusion

When performing joint state-parameter estimation including correlations in the background error covariance matrix, between parameter and state variables, improves our forecast after assimilation significantly in comparison to using a diagonal representation of $\mathbf{B}$. Specifying serial correlations between observation errors in $\hat{\mathbf{R}}$ also improves our forecast, we expect these correlations to have a greater impact when assimilating more than one data stream. When including both parameter-state correlations in $\mathbf{B}$ and time correlations between observation errors in $\hat{\mathbf{R}}$ and assimilating only a single year of NEE observations we can forecast 14 years of NEE observations with a root-mean square error of $2.38\text{gCm}^{-2}\text{day}^{-1}$. This is a significant reduction in error from the results when using a $\mathbf{B}$ and $\hat{\mathbf{R}}$ with no specified correlations of $4.22\text{gCm}^{-2}\text{day}^{-1}$.

6 Acknowledgements

Luke, FR, NERC, NCEO, (Which are needed? How to do this?)

References

C. Bacour, P. Peylin, N. MacBean, P. J. Rayner, F. Delage, F. Chevallier, M. Weiss, J. Demarty, D. Santaren, F. Baret, D. Berveiller, E. Dufrêne, and P. Prunet. Joint assimilation of eddy-covariance flux measurements and FAPAR products over temperate forests within a process-oriented biosphere model. *Journal of Geophysical Research: Biogeosciences*, pages n/a–n/a, 2015. ISSN 21698953. doi: 10.1002/2015JG002966. URL `http://doi.wiley.com/10.1002/2015JG002966`.

Dennis Baldocchi. Turner review no. 15.'breathing'of the terrestrial biosphere: lessons learned from a global network of carbon dioxide flux measurement systems. *Australian Journal of Botany*, 56(1):1–26, 2008.

Dennis Baldocchi, Cove Sturtevant, and Fluxnet Contributors. Does day and night sampling reduce spurious correlation between canopy photosynthesis and ecosystem respiration? *Agricultural and Forest Meteorology*, 207:117–126, 2015. ISSN 01681923. doi: 10.1016/j.agrformet.2015.03.010. URL `http://linkinghub.elsevier.com/retrieve/pii/S016819231500088X`.

Ross N Bannister. A review of forecast error covariance statistics in atmospheric variational data assimilation. i: Characteristics and measurements of forecast error covariances. *Quarterly Journal of the Royal Meteorological Society*, 134(637):1951–1970, 2008.

Peter Bauer, Alan Thorpe, and Gilbert Brunet. The quiet revolution of numerical weather prediction. *Nature*, 525(7567):47–55, 2015.

A. A. Bloom and M. Williams. Constraining ecosystem carbon dynamics in a data-limited world: integrating ecological "common sense" in a modeldata fusion framework. *Biogeosciences*, 12(5):1299–1315, 2015. ISSN 1726-4189. doi: 10.5194/bg-12-1299-2015. URL http://www.biogeosciences.net/12/1299/2015/.

Bobby H Braswell, William J Sacks, Ernst Linder, and David S Schimel. Estimating diurnal to annual ecosystem parameters by synthesis of a carbon flux model with eddy covariance net ecosystem exchange observations. *Global Change Biology*, 11(2):335–355, 2005.

Philippe Ciais, Christopher Sabine, Govindasamy Bala, Laurent Bopp, Victor Brovkin, Josep Canadell, Abha Chhabra, Ruth DeFries, James Galloway, Martin Heimann, et al. Carbon and other biogeochemical cycles. In *Climate change 2013: the physical science basis. Contribution of Working Group I to the Fifth Assessment Report of the Intergovernmental Panel on Climate Change*, pages 465–570. Cambridge University Press, 2014.

Roger Daley. The Effect of Serially Correlated Observation and Model Error on Atmospheric Data Assimilation, 1992. ISSN 0027-0644.

DP Dee, SM Uppala, AJ Simmons, Paul Berrisford, P Poli, S Kobayashi, U Andrae, MA Balmaseda, G Balsamo, P Bauer, et al. The era-interim reanalysis: Configuration and performance of the data assimilation system. *Quarterly Journal of the Royal Meteorological Society*, 137(656):553–597, 2011.

Sylvain Delahaies, Ian Roulstone, and Nancy Nichols. A regularization of the carbon cycle data-fusion problem. In *EGU General Assembly Conference Abstracts*, volume 15, page 4087, 2013.

Gérald Desroziers, Loic Berre, Bernard Chapnik, and Paul Poli. Diagnosis of observation, background and analysis-error statistics in observation space. *Quarterly Journal of the Royal Meteorological Society*, 131(613):3385–3396, 2005.

Jean-françois Exbrayat, T Luke Smallman, A Anthony Bloom, and Mathew Williams. Using a data-assimilation system to assess the influence of fire on simulated carbon fluxes and plant traits for the Australian continent. *EGU General Assembly*, 17:6421, 2015.

Andrew Fox, Mathew Williams, Andrew D Richardson, David Cameron, Jeffrey H Gove, Tristan Quaife, Daniel Ricciuto, Markus Reichstein, Enrico Tomelleri, Cathy M Trudinger, et al. The reflex project: comparing different algorithms and implementations for the inversion of a terrestrial ecosystem model against eddy covariance data. *Agricultural and Forest Meteorology*, 149(10):1597–1615, 2009.

Melina A. Freitag, Nancy K. Nichols, and Chris J. Budd. L1-regularisation for ill-posed problems in variational data assimilation. *Pamm*, 10(1):665–668, 2010. ISSN 16177061. doi: 10.1002/pamm.201010324. URL http://doi.wiley.com/10.1002/pamm.201010324.

S.B. Healy and A.A. White. Use of discrete Fourier transforms in the 1D-Var retrieval problem. *Quarterly Journal of the Royal Meteorological Society*, 131(605):63–72, jan 2005. ISSN 00359009. doi: 10.1256/qj.03.193. URL http://doi.wiley.com/10.1256/qj.03.193.

Heikki Järvinen, Erik Andersson, and François Bouttier. Variational assimilation of time sequences of surface observations with serially correlated errors. *Tellus A*, 51(4):469–488, 1999.

Eugenia Kalnay. *Atmospheric modeling, data assimilation, and predictability*. Cambridge university press, 2003.

T. Kaminski, W. Knorr, G. Schürmann, M. Scholze, P. J. Rayner, S. Zaehle, S. Blessing, W. Dorigo, V. Gayler, R. Giering, N. Gobron, J. P. Grant, M. Heimann, a. Hooker-Stroud, S. Houweling, T. Kato,

J. Kattge, D. Kelley, S. Kemp, E. N. Koffi, C. Köstler, P. P. Mathieu, B. Pinty, C. H. Reick, C. Rödenbeck, R. Schnur, K. Scipal, C. Sebald, T. Stacke, a. Terwisscha Van Scheltinga, M. Vossbeck, H. Widmann, and T. Ziehn. The BETHY/JSBACH Carbon Cycle Data Assimilation System: Experiences and challenges. *Journal of Geophysical Research: Biogeosciences*, 118(4):1414–1426, 2013. ISSN 21698961. doi: 10.1002/jgrg.20118.

G. Krinner, Nicolas Viovy, Nathalie de Noblet-Ducoudré, Jérôme Ogée, Jan Polcher, Pierre Friedlingstein, Philippe Ciais, Stephen Sitch, and I. Colin Prentice. A dynamic global vegetation model for studies of the coupled atmosphere-biosphere system. *Global Biogeochemical Cycles*, 19(1):1–33, 2005. ISSN 08866236. doi: 10.1029/2003GB002199.

A. S. Lawless, M.J.P. Cullen, M. A. Freitag, S. Kindermann, and R. Scheichl. *Variational data assimilation for very large environmental problems. In Large Scale Inverse Problems: Computational Methods and Applications in the Earth Sciences*. De Gruyter, 2013.

Yong Li, I. Michael Navon, Weiyu Yang, Xiaolei Zou, J. R. Bates, S. Moorthi, and R. W. Higgins. Four-Dimensional Variational Data Assimilation Experiments with a Multilevel Semi-Lagrangian Semi-Implicit General Circulation Model. *Monthly Weather Review*, 122(5):966–983, may 1994. ISSN 0027-0644. doi: 10.1175/1520-0493(1994)122¡0966:FDVDAE¿2.0.CO;2. URL `http://journals.ametsoc.org/doi/abs/10.1175/1520-0493(1994)122%3C0966:FDVDAE%3E2.0.CO%3B2`.

LI-COR, Inc. *EddyPro 6 Help and User's Guide*. LI-COR, Inc. Lincoln, NE., 2015.

Andrew C Lorenc and F Rawlins. Why does 4d-var beat 3d-var? *Quarterly Journal of the Royal Meteorological Society*, 131(613):3247–3257, 2005.

I. M. Navon, X. Zou, J. Derber, and J. Sela. Variational Data Assimilation with an Adiabatic Version of the NMC Spectral Model. *Monthly Weather Review*, 120(7):1433–1446, jul 1992. ISSN 0027-0644. doi: 10.1175/1520-0493(1992)120¡1433:VDAWAA¿2.0.CO;2. URL `http://journals.ametsoc.org/doi/abs/10.1175/1520-0493(1992)120%3C1433%3AVDAWAA%3E2.0.CO%3B2`.

IM Navon. Practical and theoretical aspects of adjoint parameter estimation and identifiability in meteorology and oceanography. *Dynamics of Atmospheres and Oceans*, 27(1):55–79, 1998.

Shuli Niu, Yiqi Luo, Michael C. Dietze, Trevor F. Keenan, Zheng Shi, Jianwei Li, and F. Stuart Chapin Iii. The role of data assimilation in predictive ecology. *Ecosphere*, 5(5):art65, 2014. ISSN 2150-8925. doi: 10.1890/ES13-00273.1. URL `http://www.esajournals.org/doi/abs/10.1890/ES13-00273.1`.

Jorge Nocedal and Stephen J Wright. *Numerical Optimization*. Springer Science & Business Media, 1999. ISBN 0387987932. URL `http://books.google.co.uk/books/about/Numerical_Optimization.html?id=epc5fX0lqRIC&pgis=1`.

D. Papale, M. Reichstein, M. Aubinet, E. Canfora, C. Bernhofer, W. Kutsch, B. Longdoz, S. Rambal, R. Valentini, T. Vesala, and D. Yakir. Towards a standardized processing of Net Ecosystem Exchange measured with eddy covariance technique: algorithms and uncertainty estimation. *Biogeosciences*, 3 (4):571–583, 2006. ISSN 1726-4189. doi: 10.5194/bg-3-571-2006.

Rona Pitman and Mark Broadmeadow. Leaf area, biomass and physiological parameterisation of ground vegetation of lowland oak woodland. *Forestry Commission, Edinburgh*, 2001.

Tristan Quaife, Philip Lewis, Martin De Kauwe, Mathew Williams, Beverly E. Law, Mathias Disney, and Paul Bowyer. Assimilating canopy reflectance data into an ecosystem model with an Ensemble Kalman Filter. *Remote Sensing of Environment*, 112(4):1347–1364, 2008. ISSN 00344257. doi: 10.1016/j.rse.2007.05.020.

Florence Rabier, H Järvinen, E Klinker, J-F Mahfouf, and A Simmons. The ecmwf operational implementation of four-dimensional variational assimilation. i: Experimental results with simplified physics. *Quarterly Journal of the Royal Meteorological Society*, 126(564):1143–1170, 2000.

F Rawlins, SP Ballard, KJ Bovis, AM Clayton, D Li, GW Inverarity, AC Lorenc, and TJ Payne. The met office global four-dimensional variational data assimilation scheme. *Quarterly Journal of the Royal Meteorological Society*, 133(623):347–362, 2007.

Andrew D Richardson, Mathew Williams, David Y Hollinger, David JP Moore, D Bryan Dail, Eric A Davidson, Neal A Scott, Robert S Evans, Holly Hughes, John T Lee, et al. Estimating parameters of a forest ecosystem c model with measurements of stocks and fluxes as joint constraints. *Oecologia*, 164 (1):25–40, 2010.

Polly J Smith, Sarah L Dance, Michael J Baines, Nancy K Nichols, and Tania R Scott. Variational data assimilation for parameter estimation: application to a simple morphodynamic model. *Ocean Dynamics*, 59(5):697–708, 2009.

Laura M. Stewart, Sarah L. Dance, and Nancy K. Nichols. Data assimilation with correlated observation errors: Experiments with a 1-D shallow water model. *Tellus, Series A: Dynamic Meteorology and Oceanography*, 65(1):1–14, 2013. ISSN 02806495. doi: 10.3402/tellusa.v65i0.19546.

Karl E. Taylor. Summarizing multiple aspects of model performance in a single diagram. *Journal of Geophysical Research*, 106(D7):7183, apr 2001. ISSN 0148-0227. doi: 10.1029/2000JD900719. URL `http://doi.wiley.com/10.1029/2000JD900719`.

Hans Verbeeck, Philippe Peylin, Cédric Bacour, Damien Bonal, Kathy Steppe, and Philippe Ciais. fluxes in Amazon forests: Fusion of eddy covariance data and the ORCHIDEE model. *Journal of Geophysical Research*, 116(G2):1–19, 2011. ISSN 0148-0227. doi: 10.1029/2010JG001544.

J. A. Waller, S. L. Dance, A. S. Lawless, N. K. Nichols, and J. R. Eyre. Representativity error for temperature and humidity using the Met Office high-resolution model. *Quarterly Journal of the Royal Meteorological Society*, 140(681):1189–1197, apr 2014. ISSN 00359009. doi: 10.1002/qj.2207. URL `http://doi.wiley.com/10.1002/qj.2207`.

Sebastian F. Walter and Lutz Lehmann. Algorithmic differentiation in Python with AlgoPy. *Journal of Computational Science*, 4(5):334–344, sep 2013. ISSN 18777503. doi: 10.1016/j.jocs.2011.10.007. URL `http://www.sciencedirect.com/science/article/pii/S1877750311001013`.

PP Weston, W Bell, and JR Eyre. Accounting for correlated error in the assimilation of high-resolution sounder data. *Quarterly Journal of the Royal Meteorological Society*, 140(685):2420–2429, 2014.

M Wilkinson, EL Eaton, MSJ Broadmeadow, and JIL Morison. Inter-annual variation of carbon uptake by a plantation oak woodland in south-eastern england. *Biogeosciences*, 9(12):5373–5389, 2012.

Mathew Williams, Edward B Rastetter, David N Fernandes, Michael L Goulden, Gaius R Shaver, and Loretta C Johnson. Predicting gross primary productivity in terrestrial ecosystems. *Ecological Applications*, 7(3):882–894, 1997.

Mathew Williams, Paul A Schwarz, Beverly E Law, James Irvine, and Meredith R Kurpius. An improved analysis of forest carbon dynamics using data assimilation. *Global Change Biology*, 11(1):89–105, 2005.

J. M. Zobitz, David J P Moore, Tristan Quaife, Bobby H. Braswell, Andrew Bergeson, Jeremy a. Anthony, and Russell K. Monson. Joint data assimilation of satellite reflectance and net ecosystem exchange data constrains ecosystem carbon fluxes at a high-elevation subalpine forest. *Agricultural and Forest Meteorology*, 195-196:73–88, 2014. ISSN 01681923. doi: 10.1016/j.agrformet.2014.04.011. URL `http://dx.doi.org/10.1016/j.agrformet.2014.04.011`.

JM Zobitz, AR Desai, DJP Moore, and MA Chadwick. A primer for data assimilation with ecological models using markov chain monte carlo (mcmc). *Oecologia*, 167(3):599–611, 2011.

Appendix

Parameter	Description	Background	Standard deviation
θ_{min}	Litter mineralisation rate (day^{-1})	$9.810e-04$	$2.030e-03$
f_{auto}	Autotrophic respiration fraction	$5.190e-01$	$1.168e-01$
f_{fol}	Fraction of GPP allocated to foliage	$1.086e-01$	$1.116e-01$
f_{roo}	Fraction of GPP allocated to fine roots	$4.844e-01$	$2.989e-01$
c_{lspan}	Determines annual leaf loss fraction	$1.200e+00$	$1.161e-01$
θ_{woo}	Woody carbon turnover rate (day^{-1})	$1.013e-04$	$1.365e-04$
θ_{roo}	Fine root carbon turnover rate (day^{-1})	$3.225e-03$	$2.930e-03$
θ_{lit}	Litter carbon turnover rate (day^{-1})	$3.442e-03$	$3.117e-03$
θ_{som}	Soil and organic carbon turnover rate (day^{-1})	$1.113e-04$	$1.181e-04$
Θ	Temperature dependance exponent factor	$4.147e-02$	$1.623e-02$
c_{eff}	Canopy efficiency parameter	$7.144e+01$	$2.042e+01$
d_{onset}	Leaf onset day	$1.158e+02$	$6.257e+00$
f_{lab}	Fraction of GPP allocated to labile carbon pool	$3.204e-01$	$1.145e-01$
c_{ronset}	Labile carbon release period	$4.134e+01$	$1.405e+01$
d_{fall}	Leaf fall day	$2.205e+02$	$3.724e+01$
c_{rfall}	Leaf-fall period	$1.168e+02$	$2.259e+01$
c_{lma}	Leaf mass per area (gCm^{-2})	$1.285e+02$	$6.410e+01$
C_{lab}	Labile carbon pool (gCm^{-2})	$1.365e+02$	$6.626e+01$
C_f	Foliar carbon pool (gCm^{-2})	$6.864e+01$	$3.590e+01$
C_r	Fine root carbon pool (gCm^{-2})	$2.838e+02$	$2.193e+02$
C_w	Above and below ground woody carbon pool (gCm^{-2})	$6.506e+03$	$7.143e+03$
C_l	Litter carbon pool (gCm^{-2})	$5.988e+02$	$5.450e+02$
C_s	Soil and organic carbon pool (gCm^{-2})	$1.936e+03$	$1.276e+03$

Table 4: Parameter values and standard deviations for background vector used in experiments.